Heterogenization of molecular cobalt catalysts in robust metal–organic frameworks for efficient photocatalytic CO 2 reduction

Srinivasulu Parshamoni, Cédric Viravaux, Marc Robert, Caroline Mellot-Draznieks, Gui Chen, Pierre Mialane, Anne Dolbecq, Julien Bonin

Heterogenization of molecular cobalt catalysts in robust metal-organic frameworks for efficient photocatalytic CO_2 reduction

Received 00th January 20xx,
Accepted 00th January 20xx

DOI: 10.1039/x0xx00000x

Srinivasulu Parshamoni,[a] Cédric Viravaux,[b] Marc Robert,*[a,c] Caroline Mellot-Draznieks,[d] Gui Chen,[e] Pierre Mialane,[b] Anne Dolbecq*[b] and Julien Bonin*[a]

A Co-quaterpyridine (Coqpy) and a Co-tris(2-pyridylmethyl)amine cobalt (CoTPA) complexes, known for their ability to reduce CO_2 to CO under visible-light irradiation in homogeneous conditions, were immobilized using the impregnation method in two different Zr-based metal-organic frameworks, UiO-67-bpydc and PCN-777, respectively. The successful synthesis of **Coqpy@UiO-67-bpydc** shows that linker deficiencies can allow catalytic complexes (Cat) to enter into the cavities of the Zr-based MOF while they would not in the defect-free MOF. The composites were characterized through solid state characterization techniques complemented by Density Functional Theory calculations in order to locate the catalysts into the MOF's pores and estimate the host/guest interactions involved. The two noble-metal free Cat@MOF composites reduce CO_2 to CO under visible-light irradiation in CH_3CN/H_2O (5:1) solutions, in the presence of $[Ru(phen)_3]^{2+}$ as solution-dissolved external photosensitizer and dimethylphenylbenzimidazoline (BIH) as electron and proton donor. CO yields, TON and selectivity reached 619 μmol g^{-1} h^{-1}, 268 and 93% respectively for **Coqpy@UiO-67-bpydc** and 368 μmol g^{-1} h^{-1}, 482 and 94% for **CoTPA@PCN-777** after 24 h solar simulated illumination. These photocatalytic studies evidenced that the composite materials are efficient, selective and recyclable and that the MOF scaffold offers a favorable environment for constant CO production rate over a long time period.

Introduction

Molecular complexes, based on noble or earth abundant metals, are largely developed as catalysts for the photochemical reduction of CO_2.[1,2] Their catalytic properties can be modulated through ligand modifications (electronic and steric tuning, through space effects such as electrostatic and H-bonding effects) and their molecular nature conveniently allows detailed mechanistic studies. Among noble-metal free molecular catalysts, 3d mononuclear complexes are particularly appealing due to their low cost but also to their good catalytic performances. However, such molecular complexes can suffer from limited stabilities under catalytic conditions and their recovery and reuse are generally made difficult due to their high solubility in polar solvents. One particularly successful strategy to address these drawbacks is to immobilize them in porous solid supports such as Metal-Organic Frameworks (MOFs) in order to form a heterogeneous Cat@MOF (Cat = molecular catalyst) catalytic system. Polyoxometalates, organometallic and coordination complexes have thus been heterogenized in MOFs for applications in the field of catalysis,[3] covering oxidation and reduction catalytic reactions, acid–base catalysis, and photo- and electrocatalysis.[4] Noticeably, the photocatalytic carbon dioxide reduction reaction has been particularly investigated these last few years,[1] the use of CO_2 representing a sustainable strategy to obtain energy-dense organic molecules (*e.g.* CO, HCOOH, CH_3OH, CH_4 ...).

In this context, we report here the preparation of new composites made of 3d molecular catalysts for photocatalytic CO_2 reduction immobilized in MOFs. Two relatively easy-to-prepare and efficient cobalt complexes, namely $[Co(qpy)(OH_2)_2]^{2+}$ (qpy = 2,2′:6′,2″:6″,2‴-quaterpyridine), abbreviated Coqpy,[5,6] and $[Co(TPA)Cl]^+$ (TPA = tris(2-pyridylmethyl)amine), abbreviated CoTPA,[7,8] (Fig. 1) have been selected as catalysts for photochemical reduction of CO_2 to CO. Among MOFs, we targeted Zr-based compounds as they represent particularly attractive hosts due to their high chemical stability.[9] Two different topologies of Zr-MOF were thus considered, PCN-777 and UiO-67, both built of Zr_6 clusters linked by tri- or di-carboxylate linkers, respectively (Fig. 1). PCN-777 displays mesoporous channels of 38 Å,[10] which is among the largest pores sizes for reported Zr-MOFs. Such large pores must

[a] Université Paris Cité, CNRS, Laboratoire d'Electrochimie Moléculaire (LEM), F-75006 Paris, France. E-mail : julien.bonin@u-paris.fr, robert@u-paris.fr
[b] Université Paris-Saclay, UVSQ, CNRS UMR 8180, Institut Lavoisier de Versailles, 78000 Versailles, France. E-mail : anne.dolbecq@uvsq.fr
[c] Institut Universitaire de France (IUF), F-75005 Paris, France.
[d] Laboratoire de Chimie des Processus Biologiques, UMR CNRS 8229, Collège de France, Sorbonne Université, PSL Research University, 11 Place Marcelin Berthelot, 75231 Paris Cedex 05, France.
[e] School of Environment and Civil Engineering, Dongguan University of Technology, Dongguan, Guangdong 523808, P. R. China.
† Electronic Supplementary Information (ESI) available: Detailed synthesis, characterizations and catalytic experiments. See DOI: 10.1039/x0xx00000x

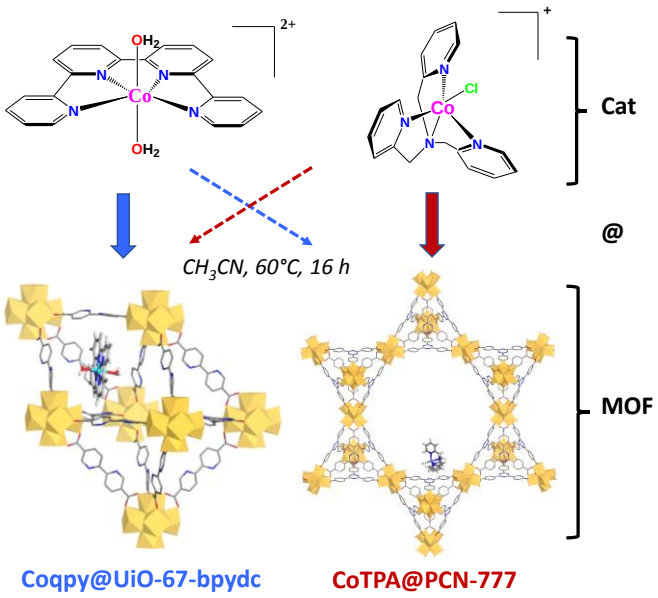

Fig. 1. Immobilization of the two cobalt molecular complexes in the two MOFs selected for the preparation of the Cat@MOF composites reported in this study; ZrO_8: yellow polyhedra, C: black spheres, N: blue spheres; positions are obtained from simulation (see text).

allow the heterogenization of bulky catalytic species such as Coqpy and CoTPA with no steric hindrance issues. Still, to our knowledge, there have been only few reports of molecular species immobilized in PCN-777 so far[11,12] and among them only one composite has been considered for catalytic applications, namely NiFe@PCN-777. This heterogeneous catalyst was synthesized by impregnation with a NiFe complex mimicking [NiFe] hydrogenase and exhibited electrocatalytic proton reduction.[13] On the other hand, UiO-67 possesses relatively small cavities (octahedral and tetrahedral cages of 18 Å and 11.5 Å internal diameters, respectively).[14] In principle, the small apertures of UiO-67's cavities should prohibit the diffusion of guest species inside the MOF and thus the use of impregnation methods for the synthesis of Cat@UiO-67 composites. Therefore, ship-in-a-bottle synthetic strategies, where the MOF is formed in presence of the catalyst,[3] have to be used. Along this line, a nickel molecular catalyst was for example encapsulated in UiO-67 via the ship-in-a-bottle method and reported for photocatalytic CO_2 reduction.[15] Alternatively, the versatility of UiO-67 also allows immobilizing molecular catalysts or photosensitizers through linker exchange whereby biphenyldicarboxylate linkers can be replaced by bipyridinedicarboxylate (bpydc) ones either by direct synthesis or post-synthetic exchange and then can be further functionalized with catalytic metal ions[16–20] or photosensitizers[15] to perform CO_2 reduction. Besides, it has also been shown that UiO-67 can easily form defective structures via missing linkers.[21] We thought that this property could be used as another strategy to allow catalytic complexes to enter into the cavities of the defective UiO-67 while they would not in the defect-free structure. In the present work, immobilization of the two efficient and selective homogeneous noble-metal free molecular catalysts, Coqpy[5] and CoTPA,[7] which possess different charges and geometries, were thus conducted in the Zr-MOFs UiO-67-bpydc and PCN-777, and their performances evaluated for CO_2 reduction under photochemical conditions.

Results and discussion

Synthesis and characterizations of the composites

The syntheses of the Cat@MOF composites were performed using the same impregnation method whereby a suspension of the MOF crystalline powder was stirred for 16 h at 60°C in an acetonitrile solution of the Co complex. Among the four attempted syntheses, only two afforded composites materials, namely **Coqpy@UiO-67-bpydc** and **CoTPA@PCN-777** (Fig. 1). These two samples were then thoroughly washed by the mixture of solvents used for the photocatalytic measurements (CH_3CN/H_2O 5:1) in order to remove amounts of Co complexes weakly bound at the surface of the MOF and thus avoid their possible leaching during catalytic tests. A slight color change, from off-white to pale orange and white to light turquoise for **Coqpy@UiO-67-bpydc** and **CoTPA@PCN-777** respectively is observed after impregnation and washing (Fig. S1a, ESI†). The morphology of the crystallites remains unchanged (Fig. S1b, ESI†). Powder X-ray diffraction patterns (PXRD) (Fig. S2, ESI†) indicate that the crystallinity of the MOF is maintained after the impregnation and washing steps. Accordingly, N_2 sorption isotherms (Fig. S3, ESI†) confirm the porous character of both the **Coqpy@UiO-67-bpydc** and **CoTPA@PCN-777** materials with a slight decrease in their surface area (1505 compared to 1617 and 1577 compared to 1792 $m^2\ g^{-1}$, respectively) due to the immobilization of the molecular catalyst. The presence of the Co complexes in the MOFs is also confirmed by SEM-EDS analysis (Table S1, ESI†) which shows a uniform distribution of the Co and Zr elements throughout the crystallites with Co/Zr_6 ratios of 0.1 and 0.04 for **Coqpy@UiO-67-bpydc** and **CoTPA@PCN-777**, respectively. EDS analysis also indicates the presence of Cl element, suggesting the co-immobilization of the ClO_4^- or Cl^- counter-ions with the Co complexes. Thermogravimetric analysis (TGA) measurements (Figs. S4 and S5 and Tables S2 and S3, ESI†) were performed to determine the total organic content of the two MOF hosts and of the resulting Cat@MOF composites. These measurements show that a large proportion of linkers are missing in UiO-67-bpydc, contrarily to what is observed for PCN-777. Interestingly, these linker deficiencies must favor the Coqpy complex to enter the UiO-67-bpydc cavities (see below). Combining the different analytical methods, we were thus able to propose the detailed following formula $[Zr_6O_4(OH)_8(H_2O)_4][bpydc]_4[Coqpy]_{0.10}(ClO_4)_{0.20}\bullet 3H_2O$ and $[Zr_6O_4(OH)_{10}(H_2O)_6][TATB]_2[CoTPA]_{0.04}Cl_{0.04}\bullet 11H_2O\bullet 2DEF$ (TATB = 4,4',4''-s-triazine-2,4,6-triyl-tribenzoate, DEF = diethylformamide) for **Coqpy@UiO-67-bpydc** and **CoTPA@PCN-777**, respectively. This corresponds to catalyst loadings of 3.17 wt% for **Coqpy@UiO-67-bpydc** and 0.74 wt% for **CoTPA@PCN-777**. Notably, the loading of CoTPA in PCN-777 is far lower than that of Coqpy in UiO-67-bpydc, suggesting

weaker host-guest interactions at play in **CoTPA@PCN-777** than in **Coqpy@UiO-67-bpydc**.

Computational investigations

Simulated annealing (SA) calculations were performed to explore the location of the guest catalyst and the nature of host-guest interactions in both **CoTPA@PCN-777** and **Coqpy@UiO-67-bpydc**. Each catalytic complex was docked into its MOF host with the counter anion(s), using a linker-defective structural model in the case of UiO-67-bpydc. Figs. 1, 2a and 2b illustrate possible favorable positions of Coqpy and CoTPA catalysts in their respective host, as obtained from dispersion-corrected DFT-D3 level geometry optimizations of the most stable conformations extracted from SA calculations. In the defective UiO-67-bpydc, missing bpydc linkers enlarge the opening of windows and thus allow access of Coqpy into the porous network of the MOF, otherwise impossible in the defect-free MOF. The most favorable site for Coqpy is found in the tetrahedral cage (Fig. 2a). The stabilization of the Coqpy complex is ensured through H···π interactions between aromatic hydrogens of qpy and benzene rings of the bpydc linkers, while one of the ClO_4^- counter-anions is stabilized through H-bond with a vicinal Zr_6-cluster. In PCN-777, CoTPA is found located in the vicinity of the MOF's organic linker, stabilized by a host-guest π- π interaction at 3.5 Å between aromatic rings of both partners in addition to interactions of the Cl^- anion with OH groups of the MOF (Fig. 2b). For both complexes, the simulations point toward the role of the counter anions in the adsorption of the complex into the MOF. Overall, the host-guest interactions estimated from DFT-D3 calculations was found rather weak (~-62 kcal/mol) for **Coqpy@UiO-67-bpydc** and even weaker (~-46 kcal/mol) for **CoTPA@PCN-777**, in agreement with experimental results for loading.

Photocatalytic properties

Photochemical assays were first performed on suspensions of **Coqpy@UiO-67-bpydc** or **CoTPA@PCN-777** composites in a mixture of acetonitrile and water (5:1) in order to explore various typical sacrificial electron donors (SEDs), *i.e.* triethylamine (TEA), triethanolamine (TEOA) and 1,3-dimethyl-2-phenyl-2,3- dihydro-1H-benzo[*d*]imidazole (BIH), in the presence of a Ru complex ($[Ru(bpy)_3]Cl_2$ or $[Ru(phen)_3](PF_6)_2$) as an external photosensitizer (PS). The solutions were saturated with CO_2 and irradiated with a solar simulator in the visible region for 24 h and CO and H_2 production measured for both composites, **Coqpy@UiO-67-bpydc** (Tables S4-S5, ESI†) and **CoTPA@PCN-777** (Tables S6-S7, ESI†). Notably, the CO production and selectivity in **Coqpy@UiO-67-bpydc** are significantly improved when using BIH (5.89 μmol, 95%) as SED instead of TEA (0.76 μmol, 33%) or TEOA (2.77 μmol, 74%) (Table S4, entries 1-3). The yield in CO is further increased to 14.8 μmol while maintaining a high selectivity (93%) when $[Ru(phen)_3](PF_6)_2$ is used as PS in place of $[Ru(bpy)_3]Cl_2$ (Table S4, entry 8). Control experiments indicate that **Coqpy@UiO-67-**

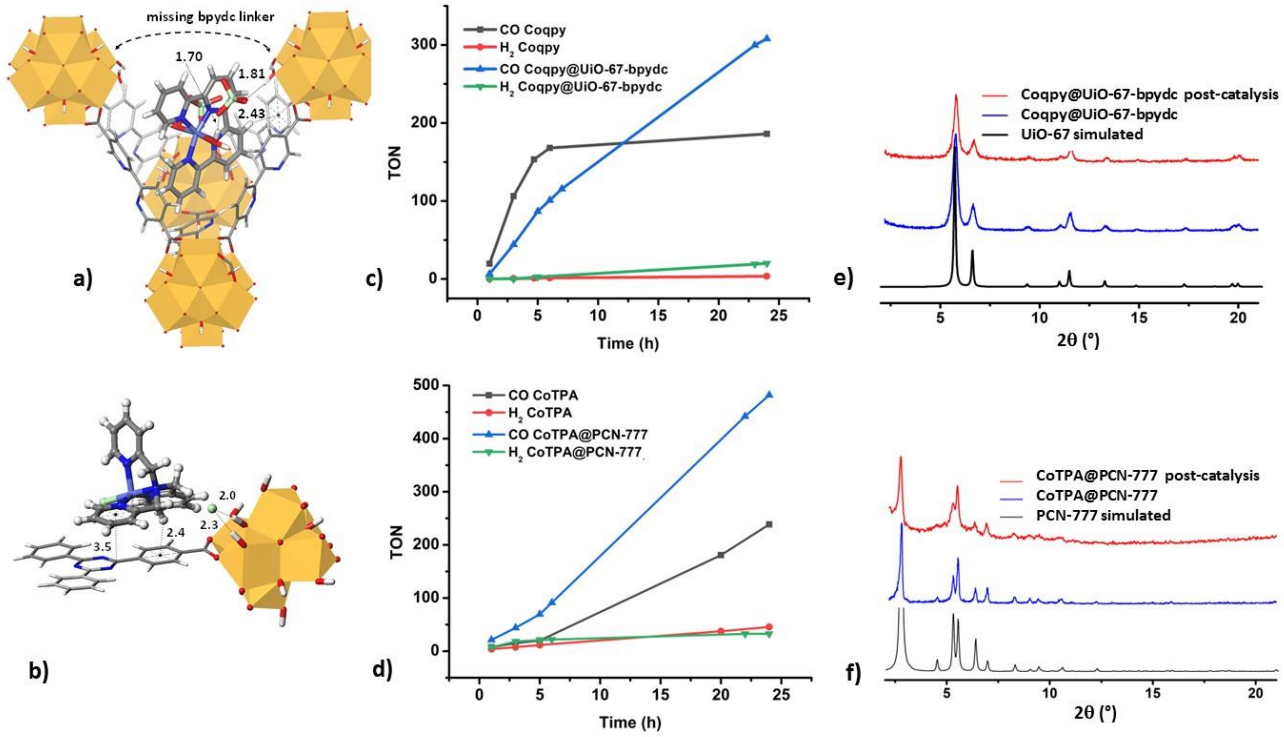

Fig. 2. View of selected favored positions of a) Coqpy in the linker defective UiO-67-bpydc and b) CoTPA in PCN-777, as extracted from SA and submitted to DFT-D3 geometry optimization. Host-guest interactions distances are given in Å. Comparison of the time profiles of CO and H_2 TONs between homogeneous catalysis and heterogeneous catalysis with c) Coqpy (1 mg) and d) CoTPA (1 mg)**,** in the presence of 1mM $[Ru(Phen)_3](PF_6)_2$ and 20 mM BIH in a CO_2-saturated CH_3CN/H_2O (2.5 mL/0.5 mL) solution**.** Powder X-ray diffraction pattern of e) **Coqpy@UiO-67-bpydc** and f) **CoTPA@PCN-777** before and after catalysis and their comparison with the simulated PXRD patterns of UiO-67 and PCN-777 respectively.

bpydc is inactive in the absence of either SED or PS (Table S4, entries 5 and 6). Similarly, the CO production is found negligible when no composite or only the complex-free UiO-67-bpydc MOF is used (Table S5, entries 2 and 5). Similar trends were observed for **CoTPA@PCN-777** for which the CO yield and selectivity go up to 7.09 μmol and 93% (Tables S6 and S7, ESI†). It can be noted that the production of formate was increased when TEOA was added to BIH as a SED (Table S5, entry 4). A similar modification in selectivity upon addition of TEOA has already been reported for Coqpy@GA (GA = graphene acid).[22] However, in this case the change in selectivity was almost complete from CO to formate. Furthermore, the presence of water was found essential for the production of CO as no activity is observed in the absence of water (Table S5, entry 3).

As shown in Fig. S7a and Table S8, using **Coqpy@UiO-67-bpydc** as heterogeneous catalyst allows an almost linear increase in the production of CO and H_2 over 24 h irradiation, with CO being produced in large excess compared to H_2. The CO turnover number (TON) and turnover frequency (TOF) thus reach 268 and 11 h^{-1} respectively, with a selectivity of 93%. Similarly, the production of CO is also almost linear with **Co-TPA@PCN-777** (Fig. S7b, Table S8, ESI†) with CO TON and TOF of 482 and 20 h^{-1} respectively and a selectivity of 94% after 24 h. The MOF scaffold thus offers a favorable environment for constant CO production rate over a long time period. Overall, the TON and selectivity values of the two composites are comparable to those of the best reported CO_2 to CO reduction Cat@MOF photosystems (Table S9, ESI†).

We then carried out additional photocatalytic CO_2 reduction assays using the two Co complexes dissolved in solution (with concentrations similar to that of the complexes in their composite counterpart) in the same conditions than with the heterogeneous systems in order to compare the photocatalytic activity of the complexes in homogeneous and heterogeneous conditions. The CO production of the Coqpy complex increased rapidly (Fig. 2c) but showed a leveling-off tendency after 6 h, reaching a TON of 186 after 24 h, far below that of the heterogeneous counterpart (268). Concerning CoTPA (Fig. 2d), the CO production remained approximately linear but was also far below that of the heterogeneous photosystem with a TON of 239 after 24 h compared to 482 reached with the heterogeneous system. Furthermore, the selectivity in CO is better in **CoTPA@PCN-777** than in the homogeneous catalytic system (94% versus 84%). These results show the beneficial effect of immobilizing the Co molecular catalysts on the efficiency, the stability or the selectivity of the photosystem.

Finally, we have also tested the recyclability of the two composites. After the photocatalytic reaction, the solid was recovered by centrifugation and reused in two additional runs. The catalysts are still active and only a slight decrease in activity is observed after the three consecutive catalytic runs (Fig. S8, ESI†). In addition, powder X-ray diffraction and SEM-EDS analyses performed on the composites after catalysis (Figs. 2e and 2f and Table S1, ESI†) show that their crystallinity and chemical compositions are maintained.

Conclusions

In conclusion, we investigated the photocatalytic CO_2 reduction performances of two Co molecular catalysts heterogenized in two different Zr-based MOFs. Among the four possible Cat@MOF combinations, two composites, **Coqpy@UiO-67-bpydc** and **CoTPA@PCN-777**, could be successfully obtained using the impregnation method. The immobilization of the Coqpy complex was made possible by a high level of linker defects in the pristine UiO-67-bpydc MOF, while computations allowed to identify favorable sites and host-guest interactions within both composites. These two materials exhibit high photocatalytic activities for CO_2 reduction with CO yields, TON and selectivity reaching 619 μmol g^{-1} h^{-1}, 268 and 93% for **Coqpy@UiO-67** and 368 μmol g^{-1} h^{-1}, 482 and 94% for **CoTPA@PCN-777** after 24 h illumination. The TON and selectivity of the heterogeneous catalysts thus exceed or are comparable to the homogeneous reference systems. Moreover, both composites could be recycled while maintaining their structural and chemical integrity. Optimization of these systems by using cobalt molecular catalysts incorporating related ligands but bearing free carboxylate groups is currently considered. It has indeed been previously shown that such groups can allow increasing the catalyst loadings via the stabilization of the catalyst through hydrogen bonds formation or their anchoring to the inorganic nodes of the MOF.[23,24] Future studies will also include the use of noble metal-free photosensitizers[25] to reach fully non-precious metal photosystems.

Experimental section

$[Co(qpy)(OH_2)_2](ClO_4)_2$[5] (Coqpy$(ClO_4)_2$), TPA,[26] $[Co(TPA)Cl]Cl$[27] ((CoTPA)Cl), PCN-777[10] and BIH[28] were synthesized according to reported procedures. All other reagents were purchased from commercial sources and used without further purification.

Materials and methods

Powder X-ray diffraction (PXRD) data were obtained on a Bruker D5000 diffractometer using Cu radiation (1.54059 Å), with a step size of 0.010° and a step time of 0.95 s. Energy dispersive spectroscopy (EDS) measurements were performed on a JEOL JSM 5800 LV

apparatus. N_2 adsorption isotherms were obtained at 77 K using a TriStar II from Micromeritics after activation with a Smart VacPrep from Micromeritics. Before the analysis, approximately 20 mg of samples were heated at 120°C under primary vacuum over 5 h. Thermogravimetry analyses (TGA) were performed on a Mettler Toledo TGA/DSC 3+, STARe System apparatus under oxygen flow (50 mL min^{-1}) at a heating rate of 3°C min^{-1} up to 700°C.

Synthesis of UiO-67-bpydc

UiO-67-bpydc was synthesised following a reported procedure[29] with slight changes. $ZrCl_4$ (24.5 mg, 0.105 mmol), 2,2-bipyridine-5,5-dicarboxylic acid (bpydc) (26 mg, 0.105 mmol) and 30 equivalents of acid modulator (glacial acetic acid, 0.2 mL) were added to a 20 mL screw cap Wheaton vial (Teflon capped). DMF (10 mL) was then added and the solution sonicated until full dispersion (10 - 30 min sonication). The solutions were then heated in a preheated oven for 24 h at 120ºC. The resulting white suspension was allowed to cool to room temperature, centrifuged at 14000 rpm and washed with DMF (2×10 mL) and MeOH (4×10 mL), resulting in a white microcrystalline powder. The powder was finally dried at 100ºC for 1h.

Synthesis of Coqpy@UiO-67-bpydc

18 mg of Coqpy$(ClO_4)_2$ was dissolved in 6 mL of CH_3CN. 30 mg of UiO-67-bpydc was added to this solution and the mixture sonicated until full dispersion (5-10 min). The solution was heated at 60ºC for 16 h under stirring, then cooled down to room temperature and centrifuged at 14000 rpm. The solid was washed by 3 x 6 mL of CH_3CN. For the final washing step, 3 mL of the solvent used for photocatalytic studies (2.5 mL of CH_3CN and 0.5 mL of H_2O) was added and the suspension stirred for 6 h at room temperature. Finally, it was centrifuged at 14000 rpm, washed with acetone and dried at 100ºC for 1 h, yielding 26 mg of off-white solid.

Synthesis of CoTPA@PCN-777

60 mg of (CoTPA)Cl was dissolved in 8 mL of CH_3CN. 40 mg of PCN-777 was added to this solution and the mixture sonicated until full dispersion (5-10 min). The solution was heated at 60ºC for 16 h under stirring, allowed to cool down to room temperature and centrifuged at 14000 rpm. The solid was washed with 3 x 6 mL of CH_3CN. For the final washing step, 3 mL of the solvent used for photocatalytic studies (2.5 mL of CH_3CN and 0.5 mL of H_2O) was added and the suspension stirred for 6 h at room temperature. Finally, it was centrifuged at 14000 rpm, washed with acetone and dried at 100ºC for 1 h, yielding 30 mg of a light turquoise solid.

Photocatalytic experiments

The photocatalytic activity of **Coqpy@UiO-67-bpydc** or **CoTPA@PCN-777** towards CO_2 reduction was measured in a CO_2 saturated mixed solution (2.5 mL of CH_3CN + 0.5 mL of H_2O) containing **Coqpy@UiO-67-bpydc** or **CoTPA@PCN-777** (1 mg), a photosensitizer ($[Ru(bpy)_3]Cl_2$ or $[Ru(Phen)_3](PF_6)_2$, 1 mM), a sacrificial electron donor (TEOA (0.2 mL), TEA (0.2 mL) or BIH (5 to 20 mM)), and irradiated at right angle with an AM 1.5G solar simulator (LCS-100, Newport) with a 400 nm cut-off filter (Schott GG400). The amount of gas products was measured by a gas chromatography set-up equipped with a high sensitivity barrier discharge ionization detector (BID-2010 Plus, Shimadzu) and liquid products by ionic chromatography (Dionex ICS-1100, Thermo Scientific).

For comparison of the activity of the composites with those of the Co complexes in homogeneous conditions, approximately the same amount of Co complexes that are immobilized in the MOFs was studied in solution. For Coqpy, 1 mg of complex was dissolved in 1 mL of CH_3CN and 60 μL of this solution was added to 3 mL of the mixture of solvent (2.5 mL CH_3CN + 0.5 mL of H_2O) used for the homogeneous photocatalytic studies. The same procedure was used for CoTPA, 1 mg of complex being dissolved in 1 mL of CH_3CN and 21 μL of this solution being added to 3 mL of the mixture of solvent (2.5 mL CH_3CN + 0.5 mL of H_2O) used for the homogeneous photocatalytic studies.

Computational methods

Force-field based conformational search: In the first step, simulated annealing (SA) calculations were used for probing the host-guest potential energy surface of the molecular catalysts (CoTPA and Coqpy) at the MOF's interface and identifying their most favorable sites into the pores or channels. Each annealing cycle consisted of 100000 independent Monte Carlo steps, initiating each energy minimization at 1000 K followed by system-cooling to 300 K, while treating the molecular catalyst as a rigid body guest and the MOF framework as the fixed-atom host. Only the position and orientation of the targeted molecular catalyst were thus sampled during SA, allowed to visit the porous volumes defined by the structural models of UiO-67 (defective) and PCN-777. In the latter case, triangular channels were excluded for authorized insertions of the guest as being not accessible from the main hexagonal channels of PCN-777. Non-bonded interactions in SA between of the molecular catalyst and the porous host were described with the *uff* forcefield[30] in which van der Waals (Lennard-Jones potentials) and electrostatic interactions were explicitly included. The atomic charges for the molecular catalyst and the MOF were calculated by the charge-equilibration method. The CoTPA net charge was fixed to +1 and compensated by one Cl^- anion, while that of the Coqpy was fixed to +2 and compensated by two ClO_4^-.

DFT-level Geometry Optimizations. DFT geometry optimizations were performed either on the fully periodic system (**Coqpy@UiO-67-bpydc**) or on a finite size model (**CoTPA@PCN-777**), which was cleaved directly from the periodic model generated over SA simulations. In the latter case, the **CoTPA@PCN-777** was designed to maintain an overall neutral charge and to preserve a good representation of the host-guest interactions occurring in the periodic model. It was also terminated with hydrogen atoms in place of the pendant linkers, while the local structure of the Zr_6 cluster in PCN-777 was modeled so that the Zr coordination was completed with -OH groups.

DFT calculations were performed in the Vienna Ab-initio Simulation Package VASP[31,32] Calculations were done using the Perdew-Burke-Ernzerhof (PBE) exchange-correlation functional.[33] The long-range weak dispersion interactions were taken into account using the semi

empirical van der Waals method of Grimme, DFT-D3.[34] The electron-ion interactions were described by the projector augmented wave (PAW) method11 in the implementation of Kresse and Joubert.[35] The Brillouin zone was sampled at the Γ-point. A plane-wave cutoff of 400 eV, for the construction of the electronic wave functions, was found to be suitable for convergence of the system. Atomic positions were optimized until the forces on all atoms were smaller than 0.02 eV $Å^{-1}$. Once the {Cat,MOF} cluster was fully optimized, the interaction energy between the Cat and the MOF was then estimated through single-point calculations of the various components, host, guest and (host, guest).

Author contributions

The project was conceived by JB, AD, PM, CMD and MR. SP, CV and GC performed the experimental work. CMD carried out the computational investigations. The manuscript was written through contributions of all authors. All authors have given approval of the final version of the manuscript.

Acknowledgements

This work was supported by CNRS, UVSQ, the Ministère de l'Enseignement Supérieur, de la Recherche et de l'Innovation. We also acknowledge financial support from the Paris Ile-de-France Region DIM 'Respore'. The calculations have been performed using the HPC national resources from GENCI (CINES/TGCC/) through Grant A0110907343.

References

1 Y.-H. Luo, L.-Z. Dong, J. Liu, S.-L. Li and Y.-Q. Lan, *Coord. Chem. Rev.*, 2019, **390**, 86–126.
2 E. Boutin, L. Merakeb, B. Ma, B. Boudy, M. Wang, J. Bonin, E. Anxolabéhère-Mallart and M. Robert, *Chem. Soc. Rev.*, 2020, **49**, 5772–5809.
3 P. Mialane, C. Mellot-Draznieks, P. Gairola, M. Duguet, Y. Benseghir, O. Oms and A. Dolbecq, *Chem. Soc. Rev.*, 2021, **50**, 6152–6220.
4 Z. Liang, C. Qu, D. Xia, R. Zou and Q. Xu, *Angew. Chem. Int. Ed.*, 2018, **57**, 9604–9633.
5 Z. Guo, S. Cheng, C. Cometto, E. Anxolabéhère-Mallart, S.-M. Ng, C.-C. Ko, G. Liu, L. Chen, M. Robert and T.-C. Lau, *J. Am. Chem. Soc.*, 2016, **138**, 9413–9416.
6 L. Chen, G. Chen, C.-F. Leung, C. Cometto, M. Robert and T.-C. Lau, *Chem. Soc. Rev.*, 2020, **49**, 7271–7283.
7 J.-W. Wang, H.-H. Huang, J.-K. Sun, T. Ouyang, D.-C. Zhong and T.-B. Lu, *ChemSusChem*, 2018, **11**, 1025–1031.
8 S. L.-F. Chan, T. L. Lam, C. Yang, S.-C. Yan and N. M. Cheng, *Chem. Commun.*, 2015, **51**, 7799–7801.
9 Y. Bai, Y. Dou, L.-H. Xie, W. Rutledge, J.-R. Li and H.-C. Zhou, *Chem. Soc. Rev.*, 2016, **45**, 2327–2367.
10 D. Feng, K. Wang, J. Su, T.-F. Liu, J. Park, Z. Wei, M. Bosch, A. Yakovenko, X. Zou and H.-C. Zhou, *Angew. Chem. Int. Ed.*, 2015, **54**, 149–154.
11 G.-B. Hu, C.-Y. Xiong, W.-B. Liang, X.-S. Zeng, H.-L. Xu, Y. Yang, L.-Y. Yao, R. Yuan and D.-R. Xiao, *ACS Appl. Mater. Interfaces*, 2018, **10**, 15913–15919.
12 J. Lee, D.-W. Lim, S. Dekura, H. Kitagawa and W. Choe, *ACS Appl. Mater. Interfaces*, 2019, **11**, 12639–12646.
13 D. Balestri, Y. Roux, M. Mattarozzi, C. Mucchino, L. Heux, D. Brazzolotto, V. Artero, C. Duboc, P. Pelagatti, L. Marchiò and M. Gennari, *Inorg. Chem.*, 2017, **56**, 14801–14808.
14 J. H. Cavka, S. Jakobsen, U. Olsbye, N. Guillou, C. Lamberti, S. Bordiga and K. P. Lillerud, *J. Am. Chem. Soc.*, 2008, **130**, 13850–13851.
15 Z.-H. Yan, B. Ma, S.-R. Li, J. Liu, R. Chen, M.-H. Du, S. Jin, G.-L. Zhuang, L.-S. Long, X.-J. Kong and L.-S. Zheng, *Sci. Bull.*, 2019, **64**, 976–985.
16 C. Wang, Z. Xie, K. E. deKrafft and W. Lin, *J. Am. Chem. Soc.*, 2011, **133**, 13445–13454.
17 M. B. Chambers, X. Wang, N. Elgrishi, C. H. Hendon, A. Walsh, J. Bonnefoy, J. Canivet, E. A. Quadrelli, D. Farrusseng, C. Mellot-Draznieks and M. Fontecave, *ChemSusChem*, 2015, **8**, 603–608.
18 H. Fei, M. D. Sampson, Y. Lee, C. P. Kubiak and S. M. Cohen, *Inorg. Chem.*, 2015, **54**, 6821–6828.
19 W.-M. Liao, J.-H. Zhang, Z. Wang, S.-Y. Yin, M. Pan, H.-P. Wang and C.-Y. Su, *J. Mater. Chem. A*, 2018, **6**, 11337–11345.
20 X. Gao, B. Guo, C. Guo, Q. Meng, J. Liang and J. Liu, *ACS Appl. Mater. Interfaces*, 2020, **12**, 24059–24065.
21 G. Kaur, S. Øien-Ødegaard, A. Lazzarini, S. M. Chavan, S. Bordiga, K. P. Lillerud and U. Olsbye, *Cryst. Growth Des.*, 2019, **19**, 4246–4251.
22 B. Ma, M. Blanco, L. Calvillo, L. Chen, G. Chen, T.-C. Lau, G. Dražić, J. Bonin, M. Robert and G. Granozzi, *J. Am. Chem. Soc.*, 2021, **143**, 8414–8425.
23 X. Wang, F. M. Wisser, J. Canivet, M. Fontecave and C. Mellot-Draznieks, *ChemSusChem*, 2018, **11**, 3315–3322.
24 S. Choi, W.-J. Jung, K. Park, S.-Y. Kim, J.-O. Baeg, C. H. Kim, H.-J. Son, C. Pac and S. O. Kang, *Acs Appl. Mater. Interfaces*, 2021, **13**, 2710–2722.
25 J. Warnan and E. Reisner, *Angew. Chem. Int. Ed.*, 2020, **59**, 17344–17354.
26 B. G. Gafford and R. A. Holwerda, *Inorg. Chem.*, 1989, **28**, 60–66.
27 C. S. Allen, C.-L. Chuang, M. Cornebise and J. W. Canary, *Inorganica Chim. Acta*, 1995, **239**, 29–37.
28 I.-S. H. Lee, E. H. Jeoung and M. M. Kreevoy, *J. Am. Chem. Soc.*, 1997, **119**, 2722–2728.
29 S. Diring, A. Carné-Sánchez, J. Zhang, S. Ikemura, C. Kim, H. Inaba, S. Kitagawa and S. Furukawa, *Chem. Sci.*, 2017, **8**, 2381–2386.
30 A. K. Rappe, C. J. Casewit, K. S. Colwell, W. A. Goddard and W. M. Skiff, *J. Am. Chem. Soc.*, 1992, **114**, 10024–10035.
31 G. Kresse and J. Furthmüller, *Comput. Mater. Sci.*, 1996, **6**, 15–50.
32 G. Kresse and J. Furthmüller, *Phys. Rev. B*, 1996, **54**, 11169–11186.
33 J. P. Perdew, K. Burke and M. Ernzerhof, *Phys. Rev. Lett.*, 1996, **77**, 3865–3868.
34 D. Andrae, U. Häußermann, M. Dolg, H. Stoll and H. Preuß, *Theor. Chim. Acta*, 1990, **77**, 123–141.
35 G. Kresse and D. Joubert, *Phys. Rev. B*, 1999, **59**, 1758–1775.